SCIENTIFIC REPORTS

OPEN

Origin of ferromagnetism in Cu-doped ZnO

Nasir Ali[1], Budhi Singh[2], Zaheer Ahmed Khan[3], Vijaya A. R. [4], Kartick Tarafder [4] & Subhasis Ghosh[1]

It is widely reported during last decade on the observation of room temperature ferromagnetism (RTFM) in doped ZnO and other transition metal oxides. However, the origin of RTFM is not understood and highly debated. While investigating the origin of RTFM, magnetic ion doped oxides should be excluded because it is not yet settled whether RTFM is intrinsic or due to the magnetic ion cluster in ZnO. Hence, it is desirable to investigate the origin of RTFM in non-magnetic ion doped ZnO and Cu-doped ZnO will be most suitable for this purpose. The important features of ferromagnetism observed in doped ZnO are (i) observation of RTFM at a doping concentration much below than the percolation threshold of wurtzite ZnO, (ii) temperature independence of magnetization and (iii) almost anhysteretic magnetization curve. We show that all these features of ferromagnetism in ZnO are due to overlapping of bound magnetic polarons (BMPs) which are created by exchange interaction between the spin of Cu^{2+} ion and spin of the localized hole due to zinc vacancy (V_{Zn}). Both the experimental and theoretical investigation show that the exchange interaction between Cu^{2+}-Cu^{2+} ions mediated by V_{Zn} is responsible for RTFM in Cu-doped ZnO.

Dilute magnetic oxides (DMOs) and dilute magnetic semiconductors (DMSs) are arguably the most interesting and intriguing magnetic materials and room temperature ferromagnetism (RTFM) in these materials is the most puzzling problem in contemporary solid state physics[1–5]. There have been innumerous reports on RTFM in ZnO films with Curie temperature (T_C) above room temperature when ZnO doped with all possible dopants, even some reports claiming RTFM in undoped ZnO[6–12]. The original idea of obtaining DMOs was to dope with only magnetic ions such as Mn, Fe, Co, Ni similar in line with studies on magnetic ions doped III–V and II–VI semiconductors[13–16]. However, this idea was seriously challenged by raising a doubt in different experimental observations whether the RTFM is at all intrinsic[17–20]. As the experimental situation is crowded with somewhat contradictory and inconsistent results, we list here the main unresolved issues in DMOs, (1) DMOs do not order magnetically similar to that in ferromagnetic materials. It is now widely accepted that the ferromagnetic order depends on the presence of defect and this leads to results based on local probes like x-ray magnetic circular dichroism and x-ray absorption near edge spectroscopy doubtful[6,21–24]. (2) RTFM can be observed in extremely dilute systems. The magnetic cations concentration responsible for ferromagnetism is much below than the cation nearest neighbor percolation threshold ($p_c \sim 0.198$) for wurtzite ZnO[25]. Hence, all the exchange mechanisms such as super-exchange and double-exchange proposed to explain ferromagnetism are doubted as the separation between two dopant impurities is very large compared to the lattice constant of ZnO[26,27]. (3) Observation of RTFM in highly resistive sample lead to irrelevance of Rudermann-Kittel-Kausya-Yosida (RKKY) mechanism for ferromagnetism which has been proposed to explain RTFM[28,29]. (4) The ubiquitous feature like temperature independent magnetization has been observed in many reports, but no explanation has been provided till date and this raises a doubt whether the proposed exchange mechanism is relevant[30,31]. (5) The magnetization curves is almost anhysteretic which again shown in all reports however not explained[21,32]. One reason behind the ambiguity in the understanding of ferromagnetism in oxide may be due to overlooking these important features of RTFM. We have considered Cu-doped ZnO as the system for solving this problem. We have avoided using magnetic ions (Fe, Co, Ni, Mn) doped ZnO to rule out any possibility of magnetic ion cluster induced ferromagnetism. Moreover, Cu or Cu cluster or any oxide of Cu is not ferromagnetic. The RTFM in Cu-doped ZnO has been reported before[33–36]. Beyond a doubt it has been established that unpaired spin on Cu-site i.e. Cu^{2+} ($3d^9$)

[1]School of Physical Sciences, Jawaharlal Nehru University, New Delhi, 110067, India. [2]Inter-University Accelerator Centre, Aruna Asaf Ali Marg, New Delhi, 110067, India. [3]Semi-Conductor Laboratory, Department of Space, S.A.S. Nagar, Punjab, India. [4]Department of Physics, National Institute of Technology Karnataka, Surathkal, 575025, India. Correspondence and requests for materials should be addressed to B.S. (email: budhisingh.jnu@gmail.com) or S.G. (email: subhasis.ghosh.jnu@gmail.com)
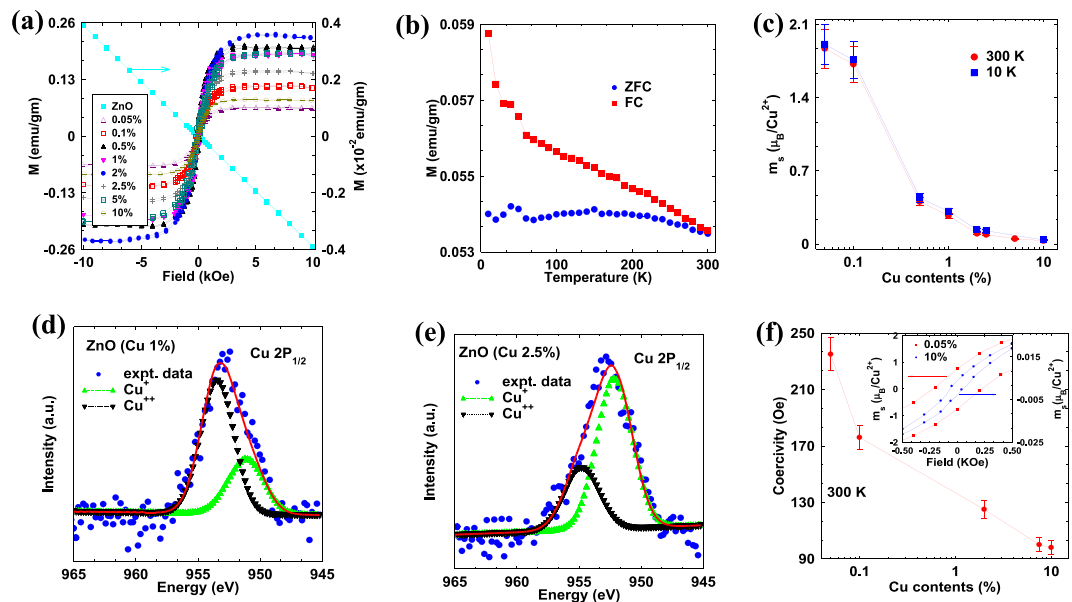
Figure 1. (**a**) Magnetization curves of ZnO doped with various concentration of Cu from 0.05% to 10%. It is clear that undoped ZnO is diamagnetic. (**b**) Zero fields cooled and field cooled magnetization of 2% Cu-doped ZnO film indicate that Curie temperature of Cu-doped ZnO is well above the room temperature. (**c**) Variation of saturated magnetic moment per Cu^{2+} ion at different doping concentration measured at 300 K and 10 K. Connecting lines are guide for eyes. (**d–e**) X-ray photoelectron spectroscopy of 1% and 2.5% Cu-doped ZnO films, respectively. (**f**) Dependence of coercivity on Cu-content in ZnO. Connecting line is guide for eyes. Inset shows the magnified hysteresis loop of 0.05% and 10% Cu-doped ZnO from −0.5 kOe to 0.5 kOe.

is responsible for ferromagnetism, however it is not known what is the long-range interaction between Cu^{2+} is responsible for ferromagnetism with T_C above room temperature. Here we present a detailed experimental and theoretical investigation to identify the long-range interaction responsible for RTFM in ZnO.

Results

Figure 1a shows the magnetization curves of the undoped and Cu-doped ZnO films with varying doping concentrations from 0.05% to 10%, measured at 300 K using a Quantum Design SQUID magnetometer. The magnetization data at 10 K is shown in Supplementary Fig. S1. The bifurcation in zero field cooled (ZFC) and field cooled (FC) magnetization *vs.* temperature for 2.5% Cu-doped ZnO film as shown in Fig. 1(b) indicates that T_C is well above the room temperature. This is very important to note that all undoped ZnO which were grown under optimized conditions are diamagnetic as shown in Fig. 1a[35,37–40]. Hence, ferromagnetism in Cu-doped ZnO must be intrinsic and not due to only defect related[11,12]. Figure 1c shows the saturated magnetic moment (m_s) per Cu^{2+} ion for different Cu concentration calculated from magnetization curves (Fig. 1a) indicating temperature independent ferromagnetic order at 300 K and 10 K. A m_s of ~1.87 μ_B/Cu^{2+} and ~1.72 μ_B/Cu^{2+} are observed in 0.05% and 0.1% Cu-doped ZnO which matches well with the spin only moment per Cu^{2+} ion in $3d^9$ configuration *i.e.*, $\mu_{eff} = g\mu_B\sqrt{S(S+1)}$ ~1.73 μ_B/Cu^{2+}[41,42]. The presence of such large value of m_s at 0.05% doping concentration, which is very small compared to p_c (~19.8%) required for long-range ferromagnetic order strongly infers the important role of intrinsic defects for long-range magnetic interaction among Cu atoms. The role of intrinsic defects on RTFM has already been emphasized in several reports[6,21,23]. The photoluminescence and absorption spectroscopy data as shown in Supplementary Fig. S3 revealed the presence of intrinsic defects in the Cu-doped ZnO through luminescence and absorption peaks at various energy levels other than the band-to-band transition. It is discussed in supplementary that below bandgap transition at ~3 eV can be attributed to zinc vacancy (V_{Zn}) and broad peak at ~2.4 eV popularly known as green luminescence is due to defect complexes. It has been shown that oxygen vacancy (V_O) and V_{Zn} are the most dominant defects in ZnO when grown under either Zn- or O-rich conditions[43,44]. At higher doping concentration, the increase in the number of Cu atoms at the hexagonal wurtzite lattice can occupy adjacent cation sites which give antiferromagnetically coupled spins and hence reduces m_s to a large extent at higher doping level (will be discussed in next section). The decrease in m_s per Cu^{2+} ion with doping is further illustrated by X-ray photoelectron spectroscopy (XPS) measurements of 1% and 2.5% Cu-doped ZnO film as shown in Fig. 1d,e. XPS data revealed the presence of mixed oxidation state of Cu^{2+} and Cu^+ ions corresponding to binding energy of 951.07 eV (952.12 eV) and 953.45 eV (954.65 eV) respectively in 1% (2.5%) Cu-doped ZnO films[33]. The +1 oxidation state represents the presence of interstitial Cu with zero magnetic moment in the ZnO lattice. From the area corresponding to each peak (Supplementary Table I), one can conclude that the number of Cu^{2+} (Cu^+) ions decreases (increases) with Cu doping.

Figure 1f shows that the coercivity of Cu-doped ZnO films at room temperature decrease with increasing Cu content. The hysteresis in magnetization curves of 0.05% and 10% Cu-doped ZnO films are shown in the inset of
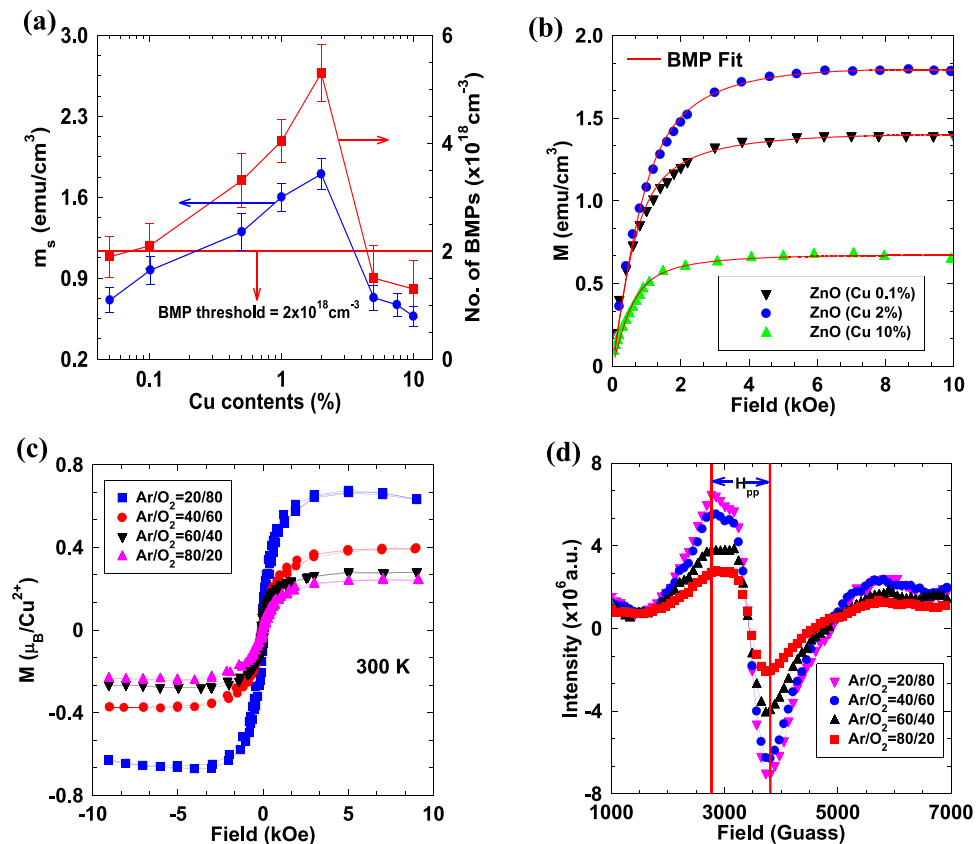
Figure 2. (**a**) Variation of saturated magnetic moment per cm³ and bound magnetic polarons concentration at various Cu doping from 0.05% to 10%. Connecting lines are guide for eyes. Horizontal line indicates the percolation threshold for bound magnetic polarons in the hexagonal wurtzite ZnO. (**b**) M–H curve fitted with BMP model. Symbols are for experimental data and the solid red line is a fit with BMP model. (**c**) Magnetization curves and (**d**) EPR spectra of 2% Cu-doped ZnO films grown at different Ar/O₂ ratio.

Fig. 1f. The magnetocrystalline anisotropy in Cu-doped ZnO film which arises mostly from spin-orbit (LS) coupling has been diminished by crystal filed splitting[45–47], resulting an almost anhysteretic magnetization curves at higher doping concentration. In addition to this, absence of ferromagnetic domains in DMO's is also responsible for anhysteretic magnetization. With Cu doping, the crystal field induced by Cu^{2+}-Cu^{2+} interaction become much larger than the spin-orbit (LS) coupling. Due to this, coupling of L and S vectors are largely broken, so that the states no longer specified by J values. Further, the $2L + 1$ sublevel belonging to a particular L which are degenerate in the free Cu^{2+} ion may now split by the crystal field and this diminishes the contribution of the orbital motion to the total magnetic moment of the Cu^{2+} ion.

Figure 2a shows m_s per cm³ as a function of the Cu content in ZnO. As the Cu content increases from 0.05% to 10%, the m_s per cm³ first increases and then decreases, reaching the maximum value of 2.48 emu/cm³ at 2% doping level. The role of intrinsic defects such as V_{Zn} and V_O to above RTFM in Cu-doped ZnO films have been investigated by depositing 2% Cu-doped ZnO films at different Ar/O₂ ratio. The Ar-deficient atmosphere creates more V_{Zn} compared to the Ar-rich atmosphere[33,43,44,48]. Figure 2c shows the magnetization data of 2% Cu-doped ZnO films grown at different Ar/O₂ ratio. Increases in m_s per Cu^{2+} ion with decreasing Ar/O₂ ratio indicates that V_{Zn} enhance the ferromagnetic order in Cu-doped ZnO. The presences of unpaired spins due to intrinsic defects within the Cu-doped ZnO films have been characterized by electron paramagnetic resonance (EPR) measurement. Figure 2d shows the EPR spectra of 2% Cu-doped ZnO films grown at different Ar/O₂ ratio. All samples show the resonance peak due to V_{Zn}^- at g = 2.01103 indicating the presence of V_{Zn}^- under both Ar-rich and deficient conditions[49–51]. The increase in the intensity of resonance amplitude in Ar-deficient conditions indicates the presence of more spins due to V_{Zn}^- available for magnetic interaction between Cu atoms. The concentration of spins can be given by the relation, $N \propto A(\Delta H_{PP})^2$[52], where N is the spin concentration, A is the amplitude, and ΔH_{PP} is the peak-to-peak width of the EPR spectrum. The obtained value of N due to V_{Zn}^- is found to be ~4 × 10¹⁸ cm⁻³. Finally, the temperature dependence resistivities of the Cu-doped ZnO films were studied and shown in Supplementary Fig. S4. Mott variable range hopping conduction in Cu-doped ZnO films indicates that the carriers are highly localized at intrinsic defect sites in Cu-doped ZnO[40,53,54]. Hence it can be concluded here that RKKY is not the origin of ferromagnetism in Cu-doped ZnO.

For the better insight of magnetic coupling mechanism responsible for RTFM, we have performed first-principle DFT simulations using the full-potential Vienna *ab*-initio simulation package (VASP)[55,56]. The
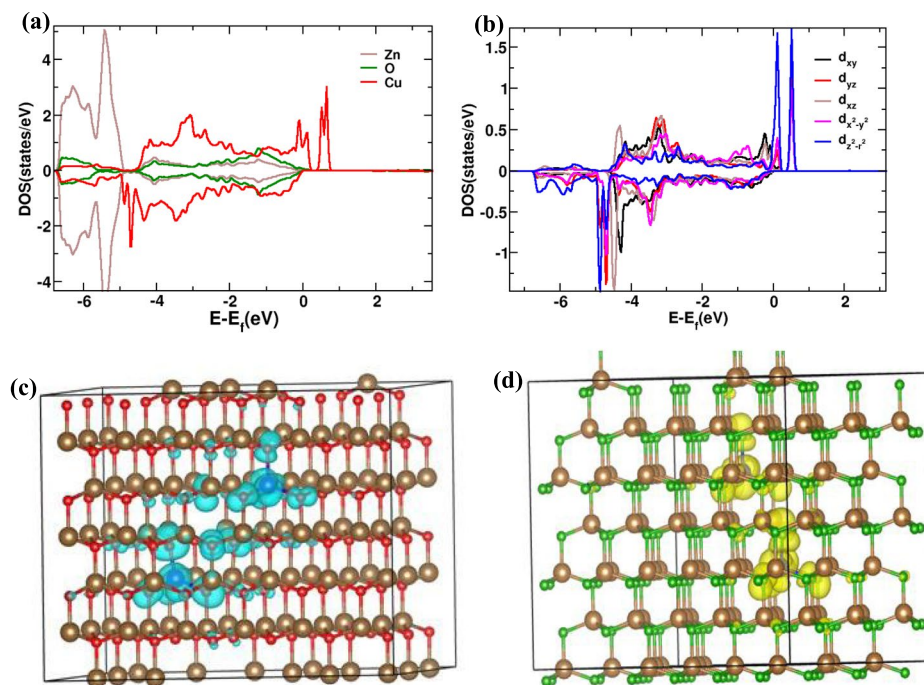
Figure 3. (**a**) Atom projected density of states in Cu-doped ZnO, (**b**) Cu-3d orbital density of states, (**c**) Significant amount of spin density distributed on neighboring O and (**d**) hole density due to V_{Zn}.

super cell used for DFT calculation is described in the methods section. The ferromagnetic stabilities were examined by comparing total energy difference (ΔE) between the ferromagnetic and antiferromagnetic configuration in different Cu-Cu separation. We found ($\Delta E = 0$), when the separations between two doped ions are 8 Å or more and the system behaves as a collection of isolated magnetic center instead of long-range ferromagnetically ordered spins. However, a weak antiferromagnetic coupling is found in case of relatively small separation distance less than 8 Å. The magnetization density overlap in two different situations is shown in Fig. 3 (a). Hence it appears that magnetic order is not possible in Cu-doped ZnO without intrinsic defect and situation is drastically changed as we introduce V_{Zn} in our calculation. For 1% V_{Zn}, our DFT results show a strong ferromagnetic coupling energy of 40~60 meV whereas the presence of V_O destroys the ferromagnetic order in Cu-doped ZnO. Our calculations indicate the partially filled Cu-e_g orbitals as shown in Fig. 3(b) giving rise to 0.64 μ_B magnetic moment on each Cu atom. Figure 3(c) shows a distribution of significant amount of spin density on neighboring O. The total magnetic moment of the supercell is 4 μ_B. The spin density of the additionally created hole due to the V_{Zn} is locally distributed between the doped Cu atoms (Fig. 3d), supporting interaction between spins on Cu atoms in relatively large distance of 7.5 Å[57]. Without Cu, V_O does not play any role in magnetism. The total magnetic moment of the unit cell remains zero in presence of V_O in ZnO. However, in presence of V_{Zn}, we found a small spin polarization with total magnetic moment in the super cell as 0.7 μ_B due to the unsaturated electrons in O atoms.

Discussion

Based on the above findings, a possible explanation for the intrinsic magnetism can be found invoking an interaction between bound magnetic polarons (BMPs)[6,58,59]. The Bohr radius associated with V_{Zn} is, $r = \varepsilon \left(\frac{m_e}{m^*} \right) a_0$, ε is the high-frequency dielectric constant, a_0 is Bohr's radius, m_e is free electron mass, m^* is the effective mass of the carrier in ZnO i.e. $m^* = 0.45 m_e$[60,61]. We have measured ε of ZnO film as a function of frequency at room temperature (Supplementary Fig. S4). Using $\varepsilon = 21$, the confinement radius of the acceptor hole is found to be ~2.4 nm. The acceptor hole on V_{Zn} creates a BMP by exchange interaction with Cu^{2+} ions. The average separation between two Cu^{2+} ions in 0.05% Cu-doped ZnO is ~2.1 nm (Supplementary Fig. S5), this means that at least two Cu^{2+} ions are available for magnetic exchange interaction in the vicinity of a V_{Zn} acceptor hole. The exchange interaction between Cu^{2+} via localized hole on V_{Zn} within a BMP takes the simple form as, $H = K \sum_i s_i \cdot (S_i + S_{i+1})$[58,59], where s and S is the spin of hole and Cu^{2+} ion, respectively. K is the magnetic exchange interaction between the spin of Cu^{2+} via localized hole is 50 meV as obtained from our DFT calculations. The single BMP can be considered as an isolated ferromagnetic identity. As the concentration of the localized hole or V_{Zn} increases; neighboring BMPs overlap and interact with each other via Cu^{2+} at Zn site. Percolation occurs when BMPs fill roughly ~14% of the space or samples size (i.e. $p_c \times$ packing fraction) as the p_c and packing fraction in ZnO is 0.198 and 0.74, respectively[25]. The percolation threshold of BMPs obtained for the appearance of long-range ferromagnetic order is (i.e. density of defects/cation density) ~5.6×10^{-5}. Using the cation density of 3.94×10^{22} cm^{-3} in ZnO[6], the defect
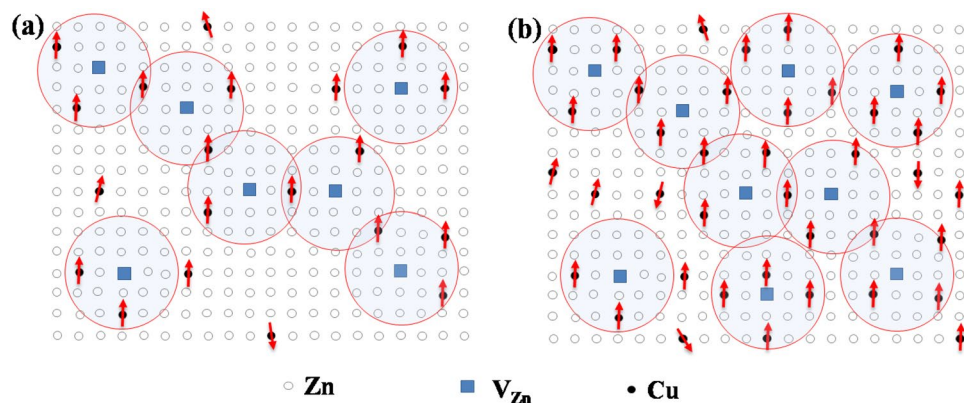
Figure 4. Schematic representation of long-range ferromagnetic order in Cu-doped ZnO mediated through bound magnetic polarons at (**a**) low doping concentration of 0.05% and (**b**) high doping concentration of 2% Cu-doped ZnO.

concentration for percolation threshold is obtained as $\sim 2 \times 10^{18}$ cm^{-3}. This concentration of V_{Zn} as obtained from EPR measurement is more than the percolation threshold facilitating a continuum path with BMPs in the sample. The horizontal line in Fig. 2a indicates the V_{Zn} concentrations for percolation threshold. The BMP concentrations can be obtained by fitting the magnetization curve using Eq.[62].

$$M = n \, m_s \mathcal{L}(x) + \mathcal{X}_m H \qquad (1)$$

where $\mathcal{L}(x)$ is the Langevin function with $x = \frac{m_{eff}H}{k_B T}$, k_B is the Boltzmann constant, m_{eff} is an effective spontaneous moment per BMP, n is the number of BMPs and $\mathcal{X}_m$ is the susceptibility of the matrix. The first term in Eq. 1 represents the contribution of the BMP's and the term $\mathcal{X}_m H$ is the matrix contribution[62]. Figure 2b shows the fitting of M-H curves of the Cu-doped ZnO films. The obtained values of BMPs at different doping concentrations are greater than the BMP$_S$ percolation threshold (as schematically shown in Fig. 4) which is required for long-range ferromagnetic order in wurtzite ZnO at room temperature (Fig. 2a). The overlapping of BMPs causes the alignment of Cu^{2+} spins (Fig. 4a), resulting ferromagnetic long chain of BMPs along the percolation path from one end of the sample to another end of sample resulting long-range ferromagnetic ordering between Cu^{2+} ions at room temperature. The corroboration of long-range ferromagnetic due to overlap of BMPs can be further established from the fact that the BMPs concentration follows the same trend as that of m_s per cm^3 for different Cu contents (Fig. 2a). Although, at low doping concentration ($\sim 0.05\%$) distance between two Cu^{2+} ions is very large but the overlap of BMPs leads to long-range ordering required for RTFM. As doping increases, more and more Cu^{2+} ions are accommodated inside BMPs with small separation resulting strong ferromagnetic order which becomes maximum at 2% doping level. After 2% doping level Cu impurities start occupying more cation sites of the wurtzite ZnO which give antiferromagnetically-coupled spins and hence reduces m_s per cm^3 to a large extent at higher doping. Similarly, at higher doping Cu^{2+} also starts occupying V_{Zn} ions resulting decrease in BMP concentration with same trend as followed by m_s per cm^3. Finally, the temperature independent of m_s in DMO's can be explained by the fact that the parameters describing BMP-BMP interaction are temperature independent in contrary to polaron percolation in DMS as described by Kaminski et al.[63]. Hence the temperature independent magnetization, as observed in our experiment and many other reports[21,30] can be explained by invoking the model put forward by Durst et al.[58], according to which the overlap region of BMP does not depend on temperature. If the overlap region depends on temperature percolation path will be broken resulting disrupting in long-range ordering responsible for ferromagnetism in Cu doped ZnO.

In conclusions, the mechanism behind RTFM at a doping concentration much below than p_c in Cu-doped ZnO has been discussed. A long-range ferromagnetic ordering has been developed, provided that there is a sufficient number of V_{Zn} higher than the number of BMP$_S$ required to achieve percolation threshold. First principle calculations show that a weak antiferromagnetic coupling is found in case of relatively small separation between Cu^{2+}-Cu^{2+} pair. However, the exchange interaction between Cu^{2+}-Cu^{2+} pair in presence of an acceptor hole due to V_{Zn} shows a strong ferromagnetic coupling energy of 50 meV at a relatively large distance of 7.5 Å. Crystal field splitting diminishes the magnetocrystalline anisotropy which results in an anhysteretic magnetization curve at higher doping level. Finally, we show that the overlapping of BMPs causes the alignment of their spins, resulting long-range ferromagnetic order in Cu-doped ZnO. The temperature independence of overlapping region between two consecutive BMPs is responsible for almost temperature independence of magnetization in Cu-doped ZnO and other DMO's.

Methods

Cu-doped ZnO films were deposited on the transparent quartz substrate by radio frequency magnetron sputtering. Sputtering targets were prepared by standard solid state route from ZnO and CuO powders (99.999%, Aldrich) weighed in stoichiometry proportions[34,64]. The pressure during deposition was maintained at 1.5×10^{-2} *mbar* under Ar/O$_2$ (60:40) atmosphere and background pressure was maintained at 1.0×10^{-7} mbar. Film

thicknesses were in the range of ~1 μm measured by Sopra GES5E spectroscopic Ellipsometer. Magnetic measurements were performed using a Quantum Design Ever Cool MPMS XL-7 superconducting quantum interference device (SQUID) magnetometer with the film orientation parallel to applied field. Grazing incidence x-ray diffraction (GIXRD) studies were performed using PANalytical Xpert Pro system with Cu K_α radiation. Optical absorption of the thin films in the range 1000–190 nm was determined using Shimadzu UV-2401PC spectrophotometer. The photoluminescence measurements were performed using an argon ion laser operating at a wavelength of 350 nm with an excitation power of 70 mW. The x-ray photoelectron spectroscopy data were recorded using an Al K_α laboratory x-ray source that was operated at 150 W at a chamber base pressure of 5×10^{-10} mbar. EPR measurements were carried out at room temperature with Bruker Model EMX MicroX system.

We have performed first-principles DFT simulations using the full-potential Vienna *ab*-initio simulation package (VASP). Projector augmented wave (PAW) potentials were used[65]. Wave functions were expanded in the plane wave basis set with kinetic energy cutoff of 500 eV. For the exchange–correlation functional, we have used GGA with Perdew and Wang (PW91) parameterization[66]. The pure ZnO has the hexagonal closed packed wurtzite structure with theoretically (DFT with GGA) calculated lattice parameters a = 3.28 Å, c = 5.33 Å with u = 0.344. To mimic the 2% doping concentration, we made a $3 \times 6 \times 3$ super cell of wurtzite-ZnO that contains 108 Zn atoms, out of which we randomly chose two Zn atoms and replaced with Cu atoms. The vacancy (~1%) was created by removing one Zn or O atom in between two Cu sites. The large unit cell geometries were further optimized. In our simulations, the forces on each of the atoms were calculated using the Hellmann-Feynman theorem and were subsequently used to perform a conjugate gradient structural relaxation. The structural optimizations were continued until the forces on the atoms converged to less than 0.01 eV/Å.

Data Availability

The data that supports the findings of this study are available from the corresponding author on reasonable request.

References

1. Dietl, T. A ten-year prospective on dilute magnetic semiconductors and oxides. *Nat. Mater.* **9**, 965–974 (2010).
2. Dietl, T. Dilute magnetic semiconductors: functional ferromagnets. *Nat. Mater.* **2**, 646–648 (2003).
3. Wurstbauer, U. *et al*. Hysteretic magnetoresistance and thermal bistability in a magnetic two-dimensional hole system. *Nat. Phys.* **6**, 955–959 (2010).
4. Chiba, D. *et al*. Electrical manipulation of magnetization reversal in a ferromagnetic semiconductor. *Science* **301**, 943–945 (2003).
5. Ohno, H. *et al*. Electric field control of ferromagnetism. *Nature* **408**, 944–946 (2000).
6. Coey, J. M. D., Venkatesaan, M. & Fitzgerald, C. B. Donor impurity band exchange in dilute ferromagnetic oxides. *Nat. Mater.* **4**, 173–179 (2005).
7. Kittilstved, K. R., Liu, W. K. & Gamelin, D. R. Electronic structure origins of polarity-dependent high-T_C ferromagnetism in oxide-diluted magnetic semiconductors. *Nat. Mater.* **5**, 291–297 (2006).
8. Ambrosio, S. D. *et al*. Competing exchange interactions in Co-doped ZnO: Departure from the superexchange picture. *Phys. Rev. B.* **86**, 035202 (2012).
9. Kundaliya, D. C. *et al*. On the origin of high-temperature ferromagnetism in the low-temperature processed Mn–Zn–O system. *Nat. Mater.* **3**, 709–714 (2004).
10. Sharma, P. *et al*. Ferromagnetism above room temperature in bulk and transparent thin films of Mn-doped ZnO. *Nat. Mater.* **2**, 673–677 (2003).
11. Wang, Q. *et al*. Vacancy-induced magnetism in ZnO thin films and nanowires. *Phys. Rev. B* **77**, 205411 (2008).
12. Kim, D., Yang, J.-H. & Hong, J. Ferromagnetism induced by Zn vacancy defect and lattice distortion in ZnO. *J.Appl. Phys.* **106**, 013908 (2009).
13. Sawicki, M. *et al*. Origin of low-temperature magnetic ordering in Ga$_{1-x}$Mn$_x$N. *Phys. Rev. B* **96**, 205204 (2012).
14. Mandal, B. *et al*. Quantum confinement: A route to enhance the Curie temperature of Mn doped GaAs. *Phys. Rev. B* **96**, 014430 (2017).
15. Litvinov, V. I. & Dugaev, V. K. Ferromagnetism in magnetically doped III–V semiconductors. *Phys. Rev. Lett.* **86**, 5593 (2001).
16. Munekata, H. *et al*. Diluted magnetic III–V semiconductors. *Phys. Rev. Lett.* **63**, 1849–1852 (1989).
17. Kim, J. Y. *et al*. Ferromagnetism Induced by Clustered Co in Co-Doped Anatase TiO$_2$ Thin Films. *Phys. Rev. Lett.* **90**, 017401 (2003).
18. Park, J. H. *et al*. Co-metal clustering as the origin of ferromagnetism in Co-doped ZnO thin films. *Appl. Phys. Lett.* **84**, 1338 (2004).
19. Cui, X. Y. *et al*. Role of Embedded Clustering in Dilute Magnetic Semiconductors: Cr Doped GaN. *Phys. Rev. Lett.* **95**, 256404 (2005).
20. Golmar, F. *et al*. Extrinsic origin of ferromagnetism in single crystalline LaAlO$_3$ substrates and oxide films. *Appl. Phys. Lett.* **92**, 262503 (2008).
21. Coey, J. M. D. *et al*. Ferromagnetism in defect-ridden oxides and related materials. *New J. Phys.* **12**, 053025 (2010).
22. Maekawa, M. *et al*. Vacancy-induced ferromagnetism in ZnO probed by spin-polarized positron annihilation spectroscopy. *Appl. Phys. Lett.* **110**, 172402 (2017).
23. Andriotis, A. N. & Menon, M. Defect-induced magnetism: Co doping and a prescription for enhanced magnetism. *Phys. Rev. B.* **87**, 155309 (2013).
24. Rana, A. K. *et al*. Search for origin of room temperature ferromagnetism properties in Ni-doped ZnO nanostructure, *ACS Appl. Mater. & Inter.* **9**, 7691–7700 (2017).
25. R. M. Zallen Physics of Amorphous solids (Wiley, New York 1983).
26. Lathiotakis, N. N., Andriotis, A. N. & Menon, M. Codoping: A possible pathway for inducing ferromagnetism in ZnO. *Phys. Rev. B.* **78**, 193311 (2008).
27. Sluiter, M. H. F. *et al*. First principles based design and experimental evidence for ZnO based ferromagnet at room temperature. *Phys. Rev. Lett.* **94**, 187204 (2005).
28. Philip, J. *et al*. Carrier-controlled ferromagnetism in transparent oxide semiconductors. *Nat. Mater.* **5**, 298–304 (2006).
29. Mukherjee, D. *et al*. Evidence for carrier-mediated magnetism in Mn-doped ZnO thin films. *Phys. Rev. B* **81**, 205202 (2010).
30. Tian, Y. *et al*. Bound magnetic polarons and p-d exchange interaction in ferromagnetic insulating Cu-doped ZnO. *App. Phys. Lett.* **98**, 162503 (2011).
31. Pal, B. & Giri, P. K. High temperature ferromagnetism and optical properties of Co doped ZnO nanoparticles. *J. Appl. Phys.* **108**, 084322 (2010).
32. Coey, J. M. D. *et al*. Charge-transfer ferromagnetism in oxide nanoparticles. *J. Phys. D: Appl. Phys.* **41**, 134012 (2008).
33. Khan, Z. A. *et al*. Green luminescence and room temperature ferromagnetism in Cu doped ZnO. *Appl. Phys. Lett.* **102**, 022105 (2013).
34. Khan, Z. A. & Ghosh, S. Robust room temperature ferromagnetism in Cu doped ZnO thin films. *Appl. Phys. Lett.* **99**, 042504 (2011).

35. Herng, T. S. *et al*. Room-Temperature Ferromagnetism of Cu-Doped ZnO Films Probed by Soft X-Ray Magnetic Circular Dichroism. *Phys. Rev. Lett.* **105**, 207201 (2010).
36. Luo, X. *et al*. Probing the magnetic profile of diluted magnetic semiconductors using polarized neutron reflectivity. *Sci. Rep.* **7**, 6341 (2017).
37. Yi, J. B. *et al*. Ferromagnetism in Dilute Magnetic Semiconductors through Defect Engineering: Li-Doped ZnO. *Phys. Rev. Lett.* **104**, 137201 (2010).
38. Chawla, S., Jayanthi, V. & Kotnala, R. K. Room-temperature ferromagnetism in Li-doped *p*-type luminescent ZnO nanorods. *Phys. Rev. B* **79**, 125204 (2009).
39. Tseng, L. T. *et al*. Intrinsic and spatially nonuniform ferromagnetism in Co-doped ZnO films. *Phys. Rev. B* **96**, 104423 (2017).
40. He, M. *et al*. Polaronic transport and magnetism in Ag-doped ZnO. *Appl. Phys. Lett.* **99**, 222511 (2011).
41. Ashcroft, N. W. & Mermin, N. D. *Solid State Physics*. (Holt, Rinehart and Winston, New York, 1976).
42. Song, C. *et al*. Giant magnetic moment in an anomalous ferromagnetic insulator: Co-doped ZnO. *Phys. Rev. B* **73**, 024405 (2006).
43. Vidya, R. *et al*. Energetics of intrinsic defects and their complexes in ZnO investigated by density functional calculations. *Phys. Rev. B* **83**, 045206 (2011).
44. Kohan, A. F. *et al*. First-principle study of native point defects in ZnO. *Phys. Rev. B* **61**, 15019 (2000).
45. Venkatesan, M. *et al*. Anisotropic ferromagnetism in substituted zinc oxide. *Phys. Rev. Lett.* **93**, 117206 (2004).
46. Ogale, S. B. *et al*. High temperature ferromagnetism with a giant magnetic moment in transparent Co-doped $SnO_{2-\delta}$. *Phys. Rev. Lett.* **91**, 077205 (2003).
47. O'Handley, R. C. Modern magnetic materials, Johm Wiley and Sons, INC. (2000).
48. Tuomisto, F., Ranki, V. & Saarinen, K. Evidence of the Zn vacancy acting as dominant acceptor in n-type ZnO. *Phys. Rev. Lett.* **20**, 205502 (2003).
49. Stehr, J. E. *et al*. Zinc-Vacancy–Donor Complex: A Crucial Compensating Acceptor in ZnO. *Phys. Rev Lett.* **2**, 021001 (2014).
50. Galland, D. & Herve, A. Temperature dependence of the ESR spectra of the zinc vacancy in ZnO. *Solid State Comm.* **14**, 953–956 (1974).
51. Galland, D. & Herve, E. S. R. Specra of the zinc vacancy in ZnO. *Phys. Lett. A* **33A**, 1–2 (1970).
52. Zhuo, S.-Y. *et al*. Ionized zinc vacancy mediated ferromagnetism in copper doped ZnO thin films. *AIP Adv.* **2**, 012184 (2012).
53. Liu, W. *et al*. A room-temperature magnetic semiconductor from a ferromagnetic metallic glass, Nat. *Comm.* **7**, 134197 (2016).
54. Thimsen, E. *et al*. High electron mobility in thin films formed via supersonic impact deposition of nanocrystals synthesized in nonthermal plasmas, Nat. *Comm.* **5**, 5822 (2014).
55. Kresse, G. & Hafner, J. *Ab* initio molecular dynamics for liquid metals. *Phys. Rev. B: Condens. Matter* **47**, 558 (1993).
56. Kresse, G. & Furthmuller, J. Efficient iterative schemes for ab initio total-energy calculations using a plane-wave basis set. *Phys. Rev. B: Condens. Matter* **54**, 11169 (1996).
57. Villegas-Lelovsky, L. *et al*. Hole-mediated ferromagnetism in coupled semimagnetic quantum dots, *Phy*. *Rev B* **84**, 075319 (2011).
58. Durst, A. C., Bhatt, R. N. & Wolff, P. A. Bound magnetic polarons interactions in insulating diluted magnetic semiconductors. *Phys. Rev. B.* **65**, 235205 (2002).
59. Wolff, P. A., Bhatt, R. N. & Durst, A. C. Polaron-polaron interactions in diluted magnetic semiconductors. *J. Appl. Phys.* **79**, 5196 (1996).
60. Sezen, H. *et al*. Evidence for photogenerated intermediate hole polarons in ZnO, Nat. *Comm.* **6**, 6901 (2015).
61. Dinges, R. *et al*. Two–photon magnetoabsorption in ZnO. *Phys. Rev. Lett.* **25**, 922 (1970).
62. McCabe, G. H. *et al*. Bound magnetic polarons in *p*-type $Cu_2Mn_{0.9}Zn_{0.1}SnS_4$. *Phys. Rev. B.* **56**, 6673 (1997).
63. Kaminski, A. & Sarma, S. D. Polaron percolation in diluted magnetic semiconductors. *Phys. Rev. Lett.* **88**, 247202 (2002).
64. Singh, B. *et al*. Highly conducting zinc oxide thin films achieved without post growth annealing. *Appl. Phys. Lett.* **97**, 241903 (2010).
65. Perdew, J. P. *et al*. Atoms, molecules, solids, and surfaces: Applications of the generalized gradient approximation for exchange and correlation. *Phys. Rev. B: Condens. Matter* **46**, 6671 (1992).
66. Kresse, G. & Joubert, D. From ultrasoft pseudo potentials to the projector augmented-wave method. *Phys. Rev. B: Condens. Matter Mater. Phys.* **59**, 1758 (1999).

Acknowledgements

Author Contributions

S.G. proposed and supervised the project. N.A., B.S. and Z.A.K. have grown films and characterized magnetic, optical and transport properties. V.A.R. and K.T. performed D.F.T. calculations. B.S. and N.A. wrote the manuscript under the guidance of S.G. and with the feedback received from other coauthors.

Additional Information

Supplementary information accompanies this paper at https://doi.org/10.1038/s41598-019-39660-x.

Competing Interests: The authors declare no competing interests.

Publisher's note: Springer Nature remains neutral with regard to jurisdictional claims in published maps and institutional affiliations.